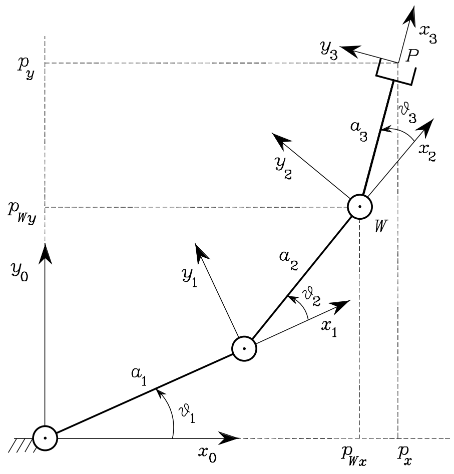

Fig. 2.20. Three-link planar arm

2.9.1 Three-link Planar Arm

Consider the three-link planar arm in Fig. 2.20, where the link frames have been illustrated. Since the revolute axes are all parallel, the simplest choice was made for all axes x_i along the direction of the relative links (the direction of x_0 is arbitrary) and all lying in the plane (x_0, y_0). In this way, all the parameters d_i are null and the angles between the axes x_i directly provide the joint variables. The DH parameters are specified in Table 2.1.

Table 2.1. DH parameters for the three-link planar arm

Link	a_i	α_i	d_i	ϑ_i
1	a_1	0	0	ϑ_1
2	a_2	0	0	ϑ_2
3	a_3	0	0	ϑ_3

Since all joints are revolute, the homogeneous transformation matrix defined in (2.52) has the same structure for each joint, i.e.,

$$\boldsymbol{A}_i^{i-1}(\vartheta_i) = \begin{bmatrix} c_i & -s_i & 0 & a_i c_i \\ s_i & c_i & 0 & a_i s_i \\ 0 & 0 & 1 & 0 \\ 0 & 0 & 0 & 1 \end{bmatrix} \qquad i = 1, 2, 3. \tag{2.62}$$

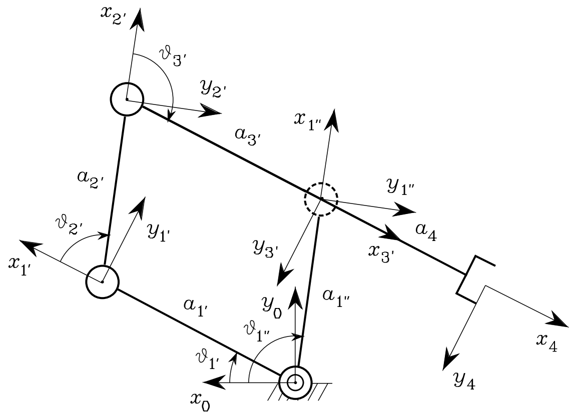

Fig. 2.21. Parallelogram arm

Computation of the direct kinematics function as in (2.50) yields

$$\boldsymbol{T}_3^0(\boldsymbol{q}) = \boldsymbol{A}_1^0\boldsymbol{A}_2^1\boldsymbol{A}_3^2 = \begin{bmatrix} c_{123} & -s_{123} & 0 & a_1c_1 + a_2c_{12} + a_3c_{123} \\ s_{123} & c_{123} & 0 & a_1s_1 + a_2s_{12} + a_3s_{123} \\ 0 & 0 & 1 & 0 \\ 0 & 0 & 0 & 1 \end{bmatrix} \tag{2.63}$$

where $\boldsymbol{q} = [\,\vartheta_1 \quad \vartheta_2 \quad \vartheta_3\,]^T$. Notice that the unit vector $\boldsymbol{z}_3^0$ of Frame 3 is aligned with $\boldsymbol{z}_0 = [\,0 \quad 0 \quad 1\,]^T$, in view of the fact that all revolute joints are parallel to axis z_0. Obviously, $p_z = 0$ and all three joints concur to determine the end-effector position in the plane of the structure. It is worth pointing out that Frame 3 does not coincide with the end-effector frame (Fig. 2.13), since the resulting approach unit vector is aligned with $\boldsymbol{x}_3^0$ and not with $\boldsymbol{z}_3^0$. Thus, assuming that the two frames have the same origin, the constant transformation

$$\boldsymbol{T}_e^3 = \begin{bmatrix} 0 & 0 & 1 & 0 \\ 0 & 1 & 0 & 0 \\ -1 & 0 & 0 & 0 \\ 0 & 0 & 0 & 1 \end{bmatrix}.$$

is needed, having taken $\boldsymbol{n}$ aligned with $\boldsymbol{z}_0$.

2.9.2 Parallelogram Arm

Consider the parallelogram arm in Fig. 2.21. A closed chain occurs where the first two joints connect Link $1'$ and Link $1''$ to Link 0, respectively. Joint 4 was selected as the cut joint, and the link frames have been established accordingly. The DH parameters are specified in Table 2.2, where $a_{1'} = a_{3'}$ and $a_{2'} = a_{1''}$ in view of the parallelogram structure.

Notice that the parameters for Link 4 are all constant. Since the joints are revolute, the homogeneous transformation matrix defined in (2.52) has

Table 2.2. DH parameters for the parallelogram arm

Link	a_i	α_i	d_i	ϑ_i
$1'$	$a_{1'}$	0	0	$\vartheta_{1'}$
$2'$	$a_{2'}$	0	0	$\vartheta_{2'}$
$3'$	$a_{3'}$	0	0	$\vartheta_{3'}$
$1''$	$a_{1''}$	0	0	$\vartheta_{1''}$
4	a_4	0	0	0

the same structure for each joint, i.e., as in (2.62) for Joints $1'$, $2'$, $3'$ and $1''$. Therefore, the coordinate transformations for the two branches of the tree are respectively:

$$\boldsymbol{A}_{3'}^{0}(\boldsymbol{q}')=\boldsymbol{A}_{1'}^{0}\boldsymbol{A}_{2'}^{1'}\boldsymbol{A}_{3'}^{2'}=\begin{bmatrix} c_{1'2'3'} & -s_{1'2'3'} & 0 & a_{1'}c_{1'}+a_{2'}c_{1'2'}+a_{3'}c_{1'2'3'} \\ s_{1'2'3'} & c_{1'2'3'} & 0 & a_{1'}s_{1'}+a_{2'}s_{1'2'}+a_{3'}s_{1'2'3'} \\ 0 & 0 & 1 & 0 \\ 0 & 0 & 0 & 1 \end{bmatrix}$$

where $\boldsymbol{q}'=[\,\vartheta_{1'}\quad\vartheta_{2'}\quad\vartheta_{3'}\,]^T$, and

$$\boldsymbol{A}_{1''}^{0}(q'')=\begin{bmatrix} c_{1''} & -s_{1''} & 0 & a_{1''}c_{1''} \\ s_{1''} & c_{1''} & 0 & a_{1''}s_{1''} \\ 0 & 0 & 1 & 0 \\ 0 & 0 & 0 & 1 \end{bmatrix}$$

where $q''=\vartheta_{1''}$. To complete, the constant homogeneous transformation for the last link is

$$\boldsymbol{A}_{4}^{3'}=\begin{bmatrix} 1 & 0 & 0 & a_4 \\ 0 & 1 & 0 & 0 \\ 0 & 0 & 1 & 0 \\ 0 & 0 & 0 & 1 \end{bmatrix}.$$

With reference to (2.59), the position constraints are ($d_{3'1''}=0$)

$$\boldsymbol{R}_{0}^{3'}(\boldsymbol{q}')\left(\boldsymbol{p}_{3'}^{0}(\boldsymbol{q}')-\boldsymbol{p}_{1''}^{0}(q'')\right)=\begin{bmatrix} 0 \\ 0 \\ 0 \end{bmatrix}$$

while the orientation constraints are satisfied independently of $\boldsymbol{q}'$ and q''. Since $a_{1'}=a_{3'}$ and $a_{2'}=a_{1''}$, two independent constraints can be extracted, i.e.,

$$\begin{aligned} a_{1'}(c_{1'}+c_{1'2'3'})+a_{1''}(c_{1'2'}-c_{1''})&=0 \\ a_{1'}(s_{1'}+s_{1'2'3'})+a_{1''}(s_{1'2'}-s_{1''})&=0. \end{aligned}$$

In order to satisfy them for any choice of $a_{1'}$ and $a_{1''}$, it must be

$$\begin{aligned} \vartheta_{2'}&=\vartheta_{1''}-\vartheta_{1'} \\ \vartheta_{3'}&=\pi-\vartheta_{2'}=\pi-\vartheta_{1''}+\vartheta_{1'} \end{aligned}$$

Therefore, the vector of joint variables is $\boldsymbol{q} = [\,\vartheta_{1'} \quad \vartheta_{1''}\,]^T$. These joints are natural candidates to be the actuated joints.[10] Substituting the expressions of $\vartheta_{2'}$ and $\vartheta_{3'}$ into the homogeneous transformation $\boldsymbol{A}^0_{3'}$ and computing the direct kinematics function as in (2.61) yields

$$\boldsymbol{T}^0_4(\boldsymbol{q}) = \boldsymbol{A}^0_{3'}(\boldsymbol{q})\boldsymbol{A}^{3'}_4 = \begin{bmatrix} -c_{1'} & s_{1'} & 0 & a_{1''}c_{1''} - a_4 c_{1'} \\ -s_{1'} & -c_{1'} & 0 & a_{1''}s_{1''} - a_4 s_{1'} \\ 0 & 0 & 1 & 0 \\ 0 & 0 & 0 & 1 \end{bmatrix}. \tag{2.64}$$

A comparison between (2.64) and (2.49) reveals that the parallelogram arm is kinematically equivalent to a two-link planar arm. The noticeable difference, though, is that the two actuated joints — providing the DOFs of the structure — are located at the base. This will greatly simplify the dynamic model of the structure, as will be seen in Sect. 7.3.3.

2.9.3 Spherical Arm

Consider the spherical arm in Fig. 2.22, where the link frames have been illustrated. Notice that the origin of Frame 0 was located at the intersection of z_0 with z_1 so that $d_1 = 0$; analogously, the origin of Frame 2 was located at the intersection between z_1 and z_2. The DH parameters are specified in Table 2.3.

Table 2.3. DH parameters for the spherical arm

Link	a_i	α_i	d_i	ϑ_i
1	0	$-\pi/2$	0	ϑ_1
2	0	$\pi/2$	d_2	ϑ_2
3	0	0	d_3	0

The homogeneous transformation matrices defined in (2.52) are for the single joints:

$$\boldsymbol{A}^0_1(\vartheta_1) = \begin{bmatrix} c_1 & 0 & -s_1 & 0 \\ s_1 & 0 & c_1 & 0 \\ 0 & -1 & 0 & 0 \\ 0 & 0 & 0 & 1 \end{bmatrix} \qquad \boldsymbol{A}^1_2(\vartheta_2) = \begin{bmatrix} c_2 & 0 & s_2 & 0 \\ s_2 & 0 & -c_2 & 0 \\ 0 & 1 & 0 & d_2 \\ 0 & 0 & 0 & 1 \end{bmatrix}$$

$$\boldsymbol{A}^2_3(d_3) = \begin{bmatrix} 1 & 0 & 0 & 0 \\ 0 & 1 & 0 & 0 \\ 0 & 0 & 1 & d_3 \\ 0 & 0 & 0 & 1 \end{bmatrix}.$$

[10] Notice that it is not possible to solve (2.64) for $\vartheta_{2'}$ and $\vartheta_{3'}$ since they are constrained by the condition $\vartheta_{2'} + \vartheta_{3'} = \pi$.

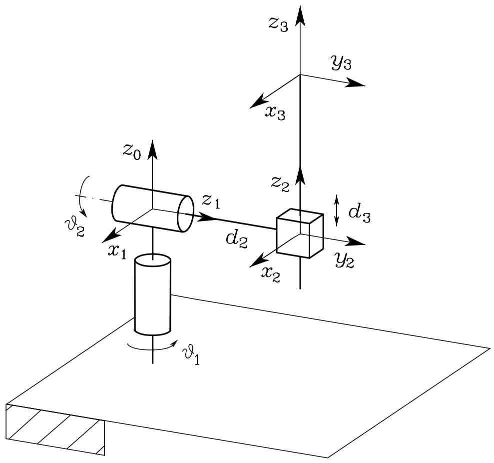

Fig. 2.22. Spherical arm

Computation of the direct kinematics function as in (2.50) yields

$$\boldsymbol{T}_3^0(\boldsymbol{q}) = \boldsymbol{A}_1^0\boldsymbol{A}_2^1\boldsymbol{A}_3^2 = \begin{bmatrix} c_1c_2 & -s_1 & c_1s_2 & c_1s_2d_3 - s_1d_2 \\ s_1c_2 & c_1 & s_1s_2 & s_1s_2d_3 + c_1d_2 \\ -s_2 & 0 & c_2 & c_2d_3 \\ 0 & 0 & 0 & 1 \end{bmatrix} \tag{2.65}$$

where $\boldsymbol{q} = [\,\vartheta_1 \quad \vartheta_2 \quad d_3\,]^T$. Notice that the third joint does not obviously influence the rotation matrix. Further, the orientation of the unit vector $\boldsymbol{y}_3^0$ is uniquely determined by the first joint, since the revolute axis of the second joint z_1 is parallel to axis y_3. Different from the previous structures, in this case Frame 3 can represent an end-effector frame of unit vectors $(\boldsymbol{n}_e, \boldsymbol{s}_e, \boldsymbol{a}_e)$, i.e., $\boldsymbol{T}_e^3 = \boldsymbol{I}_4$.

2.9.4 Anthropomorphic Arm

Consider the anthropomorphic arm in Fig. 2.23. Notice how this arm corresponds to a two-link planar arm with an additional rotation about an axis of the plane. In this respect, the parallelogram arm could be used in lieu of the two-link planar arm, as found in some industrial robots with an anthropomorphic structure.

The link frames have been illustrated in the figure. As for the previous structure, the origin of Frame 0 was chosen at the intersection of z_0 with z_1 ($d_1 = 0$); further, z_1 and z_2 are parallel and the choice of axes x_1 and x_2 was made as for the two-link planar arm. The DH parameters are specified in Table 2.4.

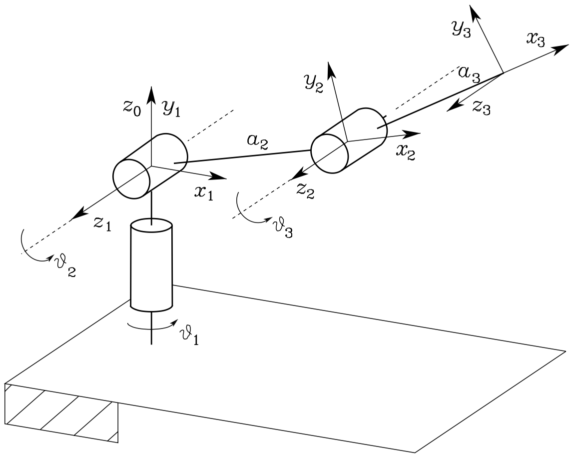

Fig. 2.23. Anthropomorphic arm

Table 2.4. DH parameters for the anthropomorphic arm

Link	a_i	α_i	d_i	ϑ_i
1	0	$\pi/2$	0	ϑ_1
2	a_2	0	0	ϑ_2
3	a_3	0	0	ϑ_3

The homogeneous transformation matrices defined in (2.52) are for the single joints:

$$\boldsymbol{A}_1^0(\vartheta_1) = \begin{bmatrix} c_1 & 0 & s_1 & 0 \\ s_1 & 0 & -c_1 & 0 \\ 0 & 1 & 0 & 0 \\ 0 & 0 & 0 & 1 \end{bmatrix}$$

$$\boldsymbol{A}_i^{i-1}(\vartheta_i) = \begin{bmatrix} c_i & -s_i & 0 & a_i c_i \\ s_i & c_i & 0 & a_i s_i \\ 0 & 0 & 1 & 0 \\ 0 & 0 & 0 & 1 \end{bmatrix} \qquad i = 2, 3.$$

Computation of the direct kinematics function as in (2.50) yields

$$\boldsymbol{T}_3^0(\boldsymbol{q}) = \boldsymbol{A}_1^0 \boldsymbol{A}_2^1 \boldsymbol{A}_3^2 = \begin{bmatrix} c_1 c_{23} & -c_1 s_{23} & s_1 & c_1(a_2 c_2 + a_3 c_{23}) \\ s_1 c_{23} & -s_1 s_{23} & -c_1 & s_1(a_2 c_2 + a_3 c_{23}) \\ s_{23} & c_{23} & 0 & a_2 s_2 + a_3 s_{23} \\ 0 & 0 & 0 & 1 \end{bmatrix} \tag{2.66}$$

where $\boldsymbol{q} = [\,\vartheta_1 \quad \vartheta_2 \quad \vartheta_3\,]^T$. Since z_3 is aligned with z_2, Frame 3 does not coincide with a possible end-effector frame as in Fig. 2.13, and a proper constant transformation would be needed.

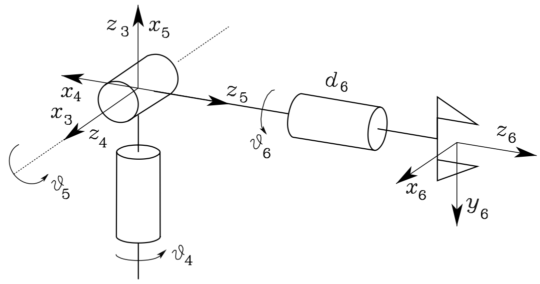

Fig. 2.24. Spherical wrist

2.9.5 Spherical Wrist

Consider a particular type of structure consisting just of the wrist of Fig. 2.24. Joint variables were numbered progressively starting from 4, since such a wrist is typically thought of as mounted on a three-DOF arm of a six-DOF manipulator. It is worth noticing that the wrist is spherical since all revolute axes intersect at a single point. Once z_3, z_4, z_5 have been established, and x_3 has been chosen, there is an indeterminacy on the directions of x_4 and x_5. With reference to the frames indicated in Fig. 2.24, the DH parameters are specified in Table 2.5.

Table 2.5. DH parameters for the spherical wrist

Link	a_i	α_i	d_i	ϑ_i
4	0	$-\pi/2$	0	ϑ_4
5	0	$\pi/2$	0	ϑ_5
6	0	0	d_6	ϑ_6

The homogeneous transformation matrices defined in (2.52) are for the single joints:

$$\boldsymbol{A}_4^3(\vartheta_4) = \begin{bmatrix} c_4 & 0 & -s_4 & 0 \\ s_4 & 0 & c_4 & 0 \\ 0 & -1 & 0 & 0 \\ 0 & 0 & 0 & 1 \end{bmatrix} \qquad \boldsymbol{A}_5^4(\vartheta_5) = \begin{bmatrix} c_5 & 0 & s_5 & 0 \\ s_5 & 0 & -c_5 & 0 \\ 0 & 1 & 0 & 0 \\ 0 & 0 & 0 & 1 \end{bmatrix}$$

$$\boldsymbol{A}_6^5(\vartheta_6) = \begin{bmatrix} c_6 & -s_6 & 0 & 0 \\ s_6 & c_6 & 0 & 0 \\ 0 & 0 & 1 & d_6 \\ 0 & 0 & 0 & 1 \end{bmatrix}.$$

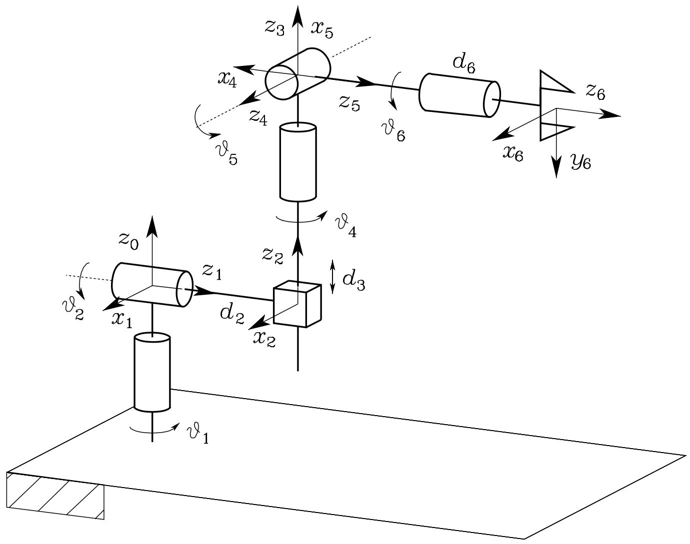

Fig. 2.25. Stanford manipulator

Computation of the direct kinematics function as in (2.50) yields

$$\boldsymbol{T}_6^3(\boldsymbol{q}) = \boldsymbol{A}_4^3\boldsymbol{A}_5^4\boldsymbol{A}_6^5 = \begin{bmatrix} c_4c_5c_6 - s_4s_6 & -c_4c_5s_6 - s_4c_6 & c_4s_5 & c_4s_5d_6 \\ s_4c_5c_6 + c_4s_6 & -s_4c_5s_6 + c_4c_6 & s_4s_5 & s_4s_5d_6 \\ -s_5c_6 & s_5s_6 & c_5 & c_5d_6 \\ 0 & 0 & 0 & 1 \end{bmatrix} \tag{2.67}$$

where $\boldsymbol{q} = [\,\vartheta_4 \quad \vartheta_5 \quad \vartheta_6\,]^T$. Notice that, as a consequence of the choice made for the coordinate frames, the block matrix $\boldsymbol{R}_6^3$ that can be extracted from $\boldsymbol{T}_6^3$ coincides with the rotation matrix of Euler angles (2.18) previously derived, that is, ϑ_4, ϑ_5, ϑ_6 constitute the set of ZYZ angles with respect to the reference frame O_3–$x_3y_3z_3$. Moreover, the unit vectors of Frame 6 coincide with the unit vectors of a possible end-effector frame according to Fig. 2.13.

2.9.6 Stanford Manipulator

The so-called Stanford manipulator is composed of a spherical arm and a spherical wrist (Fig. 2.25). Since Frame 3 of the spherical arm coincides with Frame 3 of the spherical wrist, the direct kinematics function can be obtained via simple composition of the transformation matrices (2.65), (2.67) of the previous examples, i.e.,

$$\boldsymbol{T}_6^0 = \boldsymbol{T}_3^0\boldsymbol{T}_6^3 = \begin{bmatrix} \boldsymbol{n}^0 & \boldsymbol{s}^0 & \boldsymbol{a}^0 & \boldsymbol{p}^0 \\ 0 & 0 & 0 & 1 \end{bmatrix}.$$

Carrying out the products yields

$$\boldsymbol{p}_6^0 = \begin{bmatrix} c_1 s_2 d_3 - s_1 d_2 + \big(c_1(c_2 c_4 s_5 + s_2 c_5) - s_1 s_4 s_5\big) d_6 \\ s_1 s_2 d_3 + c_1 d_2 + \big(s_1(c_2 c_4 s_5 + s_2 c_5) + c_1 s_4 s_5\big) d_6 \\ c_2 d_3 + (-s_2 c_4 s_5 + c_2 c_5) d_6 \end{bmatrix} \tag{2.68}$$

for the end-effector position, and

$$\begin{aligned} \boldsymbol{n}_6^0 &= \begin{bmatrix} c_1\big(c_2(c_4c_5c_6 - s_4s_6) - s_2s_5c_6\big) - s_1(s_4c_5c_6 + c_4s_6) \\ s_1\big(c_2(c_4c_5c_6 - s_4s_6) - s_2s_5c_6\big) + c_1(s_4c_5c_6 + c_4s_6) \\ -s_2(c_4c_5c_6 - s_4s_6) - c_2s_5c_6 \end{bmatrix} \\ \boldsymbol{s}_6^0 &= \begin{bmatrix} c_1\big(-c_2(c_4c_5s_6 + s_4c_6) + s_2s_5s_6\big) - s_1(-s_4c_5s_6 + c_4c_6) \\ s_1\big(-c_2(c_4c_5s_6 + s_4c_6) + s_2s_5s_6\big) + c_1(-s_4c_5s_6 + c_4c_6) \\ s_2(c_4c_5s_6 + s_4c_6) + c_2s_5s_6 \end{bmatrix} \\ \boldsymbol{a}_6^0 &= \begin{bmatrix} c_1(c_2c_4s_5 + s_2c_5) - s_1s_4s_5 \\ s_1(c_2c_4s_5 + s_2c_5) + c_1s_4s_5 \\ -s_2c_4s_5 + c_2c_5 \end{bmatrix} \end{aligned} \tag{2.69}$$

for the end-effector orientation.

A comparison of the vector $\boldsymbol{p}_6^0$ in (2.68) with the vector $\boldsymbol{p}_3^0$ in (2.65) relative to the sole spherical arm reveals the presence of additional contributions due to the choice of the origin of the end-effector frame at a distance d_6 from the origin of Frame 3 along the direction of $\boldsymbol{a}_6^0$. In other words, if it were $d_6 = 0$, the position vector would be the same. This feature is of fundamental importance for the solution of the inverse kinematics for this manipulator, as will be seen later.

2.9.7 Anthropomorphic Arm with Spherical Wrist

A comparison between Fig. 2.23 and Fig. 2.24 reveals that the direct kinematics function cannot be obtained by multiplying the transformation matrices $\boldsymbol{T}_3^0$ and $\boldsymbol{T}_6^3$, since Frame 3 of the anthropomorphic arm cannot coincide with Frame 3 of the spherical wrist.

Direct kinematics of the entire structure can be obtained in two ways. One consists of interposing a constant transformation matrix between $\boldsymbol{T}_3^0$ and $\boldsymbol{T}_6^3$ which allows the alignment of the two frames. The other refers to the Denavit–Hartenberg operating procedure with the frame assignment for the entire structure illustrated in Fig. 2.26. The DH parameters are specified in Table 2.6.

Since Rows 3 and 4 differ from the corresponding rows of the tables for the two single structures, the relative homogeneous transformation matrices $\boldsymbol{A}_3^2$ and $\boldsymbol{A}_4^3$ have to be modified into

$$\boldsymbol{A}_3^2(\vartheta_3) = \begin{bmatrix} c_3 & 0 & s_3 & 0 \\ s_3 & 0 & -c_3 & 0 \\ 0 & 1 & 0 & 0 \\ 0 & 0 & 0 & 1 \end{bmatrix} \qquad \boldsymbol{A}_4^3(\vartheta_4) = \begin{bmatrix} c_4 & 0 & -s_4 & 0 \\ s_4 & 0 & c_4 & 0 \\ 0 & -1 & 0 & d_4 \\ 0 & 0 & 0 & 1 \end{bmatrix}$$

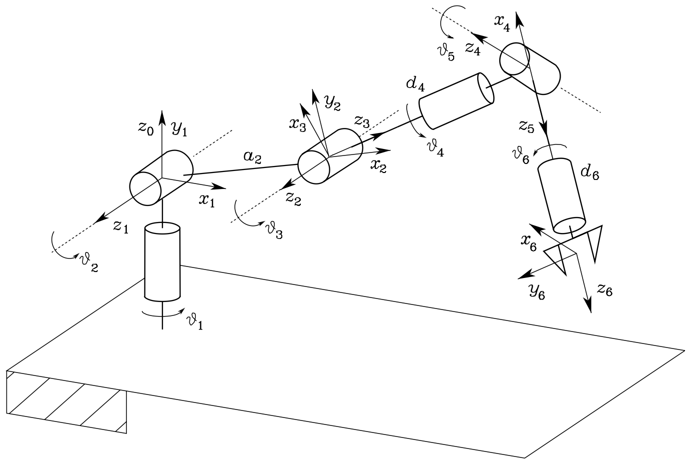

Fig. 2.26. Anthropomorphic arm with spherical wrist

Table 2.6. DH parameters for the anthropomorphic arm with spherical wrist

Link	a_i	α_i	d_i	ϑ_i
1	0	$\pi/2$	0	ϑ_1
2	a_2	0	0	ϑ_2
3	0	$\pi/2$	0	ϑ_3
4	0	$-\pi/2$	d_4	ϑ_4
5	0	$\pi/2$	0	ϑ_5
6	0	0	d_6	ϑ_6

while the other transformation matrices remain the same. Computation of the direct kinematics function leads to expressing the position and orientation of the end-effector frame as:

$$\boldsymbol{p}_6^0 = \begin{bmatrix} a_2c_1c_2 + d_4c_1s_{23} + d_6\big(c_1(c_{23}c_4s_5 + s_{23}c_5) + s_1s_4s_5\big) \\ a_2s_1c_2 + d_4s_1s_{23} + d_6\big(s_1(c_{23}c_4s_5 + s_{23}c_5) - c_1s_4s_5\big) \\ a_2s_2 - d_4c_{23} + d_6(s_{23}c_4s_5 - c_{23}c_5) \end{bmatrix} \tag{2.70}$$

and

$$\begin{aligned} \boldsymbol{n}_6^0 &= \begin{bmatrix} c_1\big(c_{23}(c_4c_5c_6 - s_4s_6) - s_{23}s_5c_6\big) + s_1(s_4c_5c_6 + c_4s_6) \\ s_1\big(c_{23}(c_4c_5c_6 - s_4s_6) - s_{23}s_5c_6\big) - c_1(s_4c_5c_6 + c_4s_6) \\ s_{23}(c_4c_5c_6 - s_4s_6) + c_{23}s_5c_6 \end{bmatrix} \\ \boldsymbol{s}_6^0 &= \begin{bmatrix} c_1\big(-c_{23}(c_4c_5s_6 + s_4c_6) + s_{23}s_5s_6\big) + s_1(-s_4c_5s_6 + c_4c_6) \\ s_1\big(-c_{23}(c_4c_5s_6 + s_4c_6) + s_{23}s_5s_6\big) - c_1(-s_4c_5s_6 + c_4c_6) \\ -s_{23}(c_4c_5s_6 + s_4c_6) - c_{23}s_5s_6 \end{bmatrix} \\ \boldsymbol{a}_6^0 &= \begin{bmatrix} c_1(c_{23}c_4s_5 + s_{23}c_5) + s_1s_4s_5 \\ s_1(c_{23}c_4s_5 + s_{23}c_5) - c_1s_4s_5 \\ s_{23}c_4s_5 - c_{23}c_5 \end{bmatrix}. \end{aligned} \tag{2.71}$$

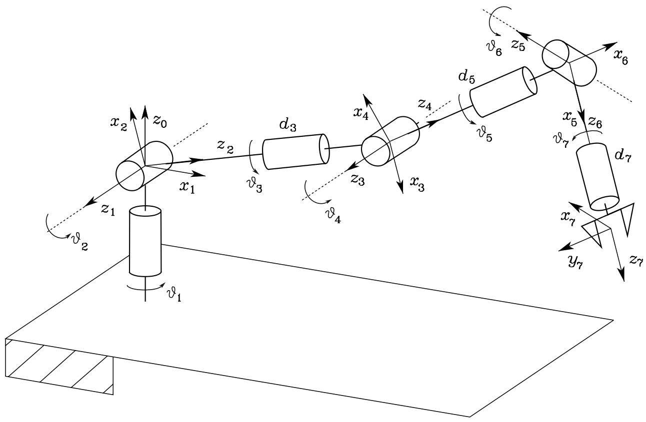

Fig. 2.27. DLR manipulator

By setting $d_6 = 0$, the position of the wrist axes intersection is obtained. In that case, the vector $\boldsymbol{p}^0$ in (2.70) corresponds to the vector $\boldsymbol{p}_3^0$ for the sole anthropomorphic arm in (2.66), because d_4 gives the length of the forearm (a_3) and axis x_3 in Fig. 2.26 is rotated by $\pi/2$ with respect to axis x_3 in Fig. 2.23.

2.9.8 DLR Manipulator

Consider the DLR manipulator, whose development is at the basis of the realization of the robot in Fig. 1.30; it is characterized by seven DOFs and as such it is inherently redundant. This manipulator has two possible configurations for the outer three joints (wrist). With reference to a spherical wrist similar to that introduced in Sect. 2.9.5, the resulting kinematic structure is illustrated in Fig. 2.27, where the frames attached to the links are evidenced.

As in the case of the spherical arm, notice that the origin of Frame 0 has been chosen so as to zero d_1. The DH parameters are specified in Table 2.7.

Table 2.7. DH parameters for the DLR manipulator

Link	a_i	α_i	d_i	ϑ_i
1	0	$\pi/2$	0	ϑ_1
2	0	$\pi/2$	0	ϑ_2
3	0	$\pi/2$	d_3	ϑ_3
4	0	$\pi/2$	0	ϑ_4
5	0	$\pi/2$	d_5	ϑ_5
6	0	$\pi/2$	0	ϑ_6
7	0	0	d_7	ϑ_7